

# A Reliable Calibration of HII Galaxies Hubble Diagram with Cosmic Chronometers and Artificial Neural Network

JIAN-CHEN ZHANG(张建臣) <sup>1,2,3,4</sup> KANG JIAO(焦康) <sup>1,2,5</sup> TINGTING ZHANG,<sup>6</sup> TONG-JIE ZHANG(张同杰) <sup>1,2,4</sup> AND  
Bo Yu(于波) <sup>4,7,8</sup>

<sup>1</sup>*Institute for Frontiers in Astronomy and Astrophysics of Beijing Normal University, Beijing 100875, China; tjzhang@bnu.edu.cn*

<sup>2</sup>*Department of Astronomy, Beijing Normal University, Beijing 100875, China*

<sup>3</sup>*College of Computer and Information Engineering, Dezhou University, Dezhou 253023, China*

<sup>4</sup>*Institute for Astronomical Science, Dezhou University, Dezhou 253023, China*

<sup>5</sup>*Dipartimento di Fisica e Astronomia “Augusto Righi”, Alma Mater Studiorum Università di Bologna, via Piero Gobetti 93/2, I-40129 Bologna, Italy*

<sup>6</sup>*College of Command and Control Engineering, PLA Army Engineering University, Nanjing 210000, China; 101101964@seu.edu.cn*

<sup>7</sup>*School of Mathematics and Big Data, Dezhou University, Dezhou 253023, China*

<sup>8</sup>*Shandong Provincial Key Laboratory of Biophysics, Institute of Biophysics, Dezhou University, Dezhou 253023, China*

## ABSTRACT

The  $L - \sigma$  relation of HII galaxies (HIIGx) calibrated by a distance indicator is a reliable standard candle for measuring the Hubble constant  $H_0$ . The most straightforward calibration technique anchors them with the first tier of distance ladders from the same galaxies. Recently another promising method that uses the cosmological model-independent Cosmic Chronometers (CC) as a calibrator has been proposed. We promote this technique by removing the assumptions about the cosmic flatness and using a non-parametric Artificial Neural Network for the data reconstruction process. We observe a correlation between the cosmic curvature density parameter and the slope of the  $L - \sigma$  relation, thereby improving the reliability of the calibration. Using the calibrated HIIGx Hubble diagram, we obtain a Type Ia Supernovae Hubble diagram free of the conventional assumption about  $H_0$ . Finally we get a value of  $H_0 = 65.9_{-2.9}^{+3.0}$  km s<sup>-1</sup> Mpc<sup>-1</sup>, which is compatible with latest Planck18 measurement.

*Keywords:* Hubble diagram(759); H II regions(694); Standard candles(1563); Hubble constant(758); Astronomy data analysis(1858); Neural networks(1933); Type Ia supernovae(1728)

## 1. INTRODUCTION

Hubble diagrams contain a wealth of information on the mass-energy content and evolutionary history of the Universe via the distance redshift relation they present. A Hubble diagram can be constructed using any astronomical source with standardizable intrinsic properties that are calibrated using known credible distance indicators. For example, Type Ia Supernovae (SNe Ia), which share the same explosion mechanism, thus have an intrinsic luminosity that can be used to measure the luminosity distance (Riess et al. 1998; Perlmutter et al. 1999). The  $E_{p,i} - E_{iso}$  correlation of Gamma-ray bursts (GRBs) has no significant redshift dependence and thus can be used to measure distance (Demianski, Marek et al. 2017). The non-linear relationship between X-ray and UV emission in quasars enables a novel, highly accurate method for estimating the absolute luminosity, converting it to standard candles (Lusso, E. & Risaliti,

G. 2017; Salvestrini, F. et al. 2019; Lusso, E. et al. 2020). Fast radio bursts (FRBs) dispersion is a convolution of the cosmic distance element and the electron density, which enables the use of these events as cosmological distance measurements (Kumar & Linder 2019).

HII galaxies (HIIGx) are massive and compact aggregates of star formation. The starburst nearly entirely dominates the total luminosity of an HIIGx. The strong correlation between the luminosity  $L(H\beta)$  in  $H\beta$  lines and the ionized gas velocity dispersion  $\sigma_v$  (Terlevich & Melnick 1981; Chávez et al. 2014; Melnick, J. et al. 2017) provides a tool for constructing the Hubble diagram and is then used to estimate  $H_0$  after calibration with the first tier of distance ladders (Chávez et al. 2012; Fernández Arenas et al. 2017). Apart from this type of local calibration, a new method was recently presented that extends to high redshifts by reconstructing Cosmic Chronometers (CC) to obtain distance information

(Wu et al. 2020). They applied the prevalent Gaussian Process (GP) (Seikel et al. 2012) reconstruction in their approach and obtained an accurate calibration of the HIIGx Hubble diagram. However, their result is based on the assumptions that the Universe is flat and the observational data are correlated by a kernel function. Removing the assumptions will further improve the reliability of this calibration method, especially for the concern that the last assumption is relatively strong.

Artificial Neural Network (ANN) is a machine learning technique that excels at regression. It has recently been broadly utilized in astronomical studies. Such as distinguishing standard and modified gravity cosmologies (Peel et al. 2019), estimating cosmological parameters (Wang et al. 2020b), simulating Cosmic Microwave background anisotropy maps (Mishra et al. 2019), creating weak lensing convergence map (Mustafa et al. 2019), discriminating cosmological models (Schmelzle et al. 2017), likelihood-free cosmological constraints (Wang et al. 2021) Etc. Wang et al. (2020a) make use of ANN in reconstructing functions of the  $H(z)$  and the  $D_L(z)$  using OHD and SNe Ia data. They prove its reliability and superiority in characterizing data uncertainties.

In this article, we propose using the ANN and CC to obtain a reliable calibration of the HIIGx Hubble diagram without any assumptions. In section 2, we illustrate the principle of calibrating the HIIGx Hubble diagram. In section 3, we describe the principle and methodology in the local measurement of  $H_0$ , specifically about using the calibrated HIIGx Hubble diagram in section 3.1 and the cross-calibrated SNe Hubble diagram in section 3.2. In section 4, we present the data used in this article and present our results. In section 5, we draw our conclusions and engage in some discussion.

## 2. CALIBRATING THE HIIGX HUBBLE DIAGRAM

The luminosity of Balmer  $H\beta$  lines that emitted in HIIGx is strongly correlated with the ionized gas velocity dispersion  $\sigma_v$  (Terlevich & Melnick 1981), since both the intensity of ionizing radiation and the value of  $\sigma_v$  grow as the starburst mass increases (Siegel et al. 2005). This correlation can be approximated by the expression in Chávez et al. (2012),

$$\lg \left[ \frac{L(H\beta)}{\text{erg s}^{-1}} \right] = \alpha \lg \left[ \frac{\sigma_v(H\beta)}{\text{km s}^{-1}} \right] + \kappa, \quad (1)$$

where  $\alpha$  and  $\kappa$  are constant coefficients in this linear relation. Due to the low dispersion of this relation observed between  $L(H\beta)$  and  $\sigma_v$ , these galaxies and local HII regions can be utilized as standard candles (Terlevich et al. 2015; Wei et al. 2016; Yennapureddy & Melia 2017; Leaf & Melia 2018).

The selection criteria ensure that the selected HIIGx are comprised of systems in which the luminosity is dominated by single and very young starbursts (less than 5 Myr in age) (Terlevich et al. 2015). Accordingly, the bolometric flux of the HIIGx can thus be regarded as primarily constituting the  $H\beta$  line. Therefore the luminosity distance- $D_L(z)$  of an HIIGx can be approximated using the luminosity  $L(H\beta)$  and flux  $F(H\beta)$  associated to the  $H\beta$  line,

$$D_L = \left[ \frac{L(H\beta)}{4\pi F(H\beta)} \right]^{1/2}, \quad (2)$$

where  $F(H\beta)$  denotes the reddening corrected  $H\beta$  flux. By the definition of distance modulus

$$\mu = 5 \lg D_L + 25, \quad (3)$$

we can obtain

$$\mu_{\text{HII}} = 2.5[\alpha \lg \sigma_v(H\beta) + \kappa - \lg F(H\beta)] - 100.2, \quad (4)$$

while the error propagation is

$$\sigma_{\mu_{\text{HII}}}^2(\alpha, z_i) = 2.5^2[(\alpha \sigma_{\lg \sigma_v})^2 + \sigma_{\lg F}^2], \quad (5)$$

where  $\sigma_{\lg \sigma_v}$  and  $\sigma_{\lg F}$  are the measurement error  $\lg \sigma_v$  and  $\lg F$  respectively.

If we can measure the  $D_L$  at the same redshift as the observed HIIGx, we are able to calibrate the slope ( $\alpha$ ) and intercept ( $\kappa$ ) of the  $L - \sigma$  relation. Locally, it is not difficult to anchor the HIIGx with reliable distance modulus determined by other distance indicators within the same galaxy, such as the period-luminosity relation of Cepheid. For a higher redshift range that the first tier of the distance ladder is not applicable, we might obtain the anchors by integrating the inverse of the Observation  $H(z)$  Data (OHD, also known as CC) across redshift,

$$\frac{D_L}{(1+z)} = \begin{cases} \frac{D_H}{\sqrt{\Omega_{k0}}} \sinh \left[ \sqrt{\Omega_{k0}} D_C / D_H \right] & \Omega_{k0} > 0 \\ D_C & \Omega_{k0} = 0 \\ \frac{D_H}{\sqrt{|\Omega_{k0}|}} \sin \left[ \sqrt{|\Omega_{k0}|} D_C / D_H \right] & \Omega_{k0} < 0 \end{cases} \quad (6)$$

where  $\Omega_{k0}$  is the curvature energy density parameter, the Hubble radius  $D_H = c/H_0$ , and the comoving distance

$$D_C = c \int_0^z \frac{dz'}{H(z')}, \quad (7)$$

$c$  denotes the speed of light, and  $H(z')$  denotes the Hubble parameter at redshift  $z'$ . If we want to get the  $D_C$  at any redshift of interest, a reconstruction based on the OHD is a prerequisite. Reconstructing  $H(z)$  would complicate the covariance propagation, therefore we choose

the same method as Wu et al. (2020) that reconstruct  $c/H(z)$ . We do the integration using

$$D_C \simeq \sum \frac{c}{H(z_i)} \Delta z_i, \quad (8)$$

which strictly holds if the redshift interval  $\Delta z_i = \frac{1}{2}(z_{i-1} - z_{i+1})$  is smaller enough. The covariance of the reconstructed data will propagate to the  $D_C$  in an approximate form of

$$\text{Cov}_{D_C}(z_i, z_j) = \sum_l^i \sum_k^j \text{Cov}\left(\frac{c}{H_k}, \frac{c}{H_l}\right) \Delta z_k \Delta z_l, \quad (9)$$

which further propagate to the covariance of  $\mu$  as

$$\text{Cov}_\mu(H_0, \Omega_{k0}; z_i, z_j) = \mathcal{C}_i \mathcal{C}_j \text{Cov}_{D_C}(z_i, z_j), \quad (10)$$

where the coefficient  $\mathcal{C}_i$  in error propagation is a function of  $\Omega_k$  and  $H_0$ ,

$$\mathcal{C}_i \frac{\ln 10}{5} = \begin{cases} \frac{\sqrt{\Omega_{k0}}}{D_H} \coth\left[\frac{\sqrt{\Omega_{k0}} D_{Ci}}{D_H}\right] & \Omega_{k0} > 0 \\ \frac{1}{D_C} & \Omega_{k0} = 0 \\ \frac{\sqrt{|\Omega_{k0}|}}{D_H} \cot\left[\frac{\sqrt{|\Omega_{k0}|} D_{Ci}}{D_H}\right] & \Omega_{k0} < 0 \end{cases}. \quad (11)$$

The HIIGx Hubble diagram can be calibrated without any assumption of the cosmological model or the geometry of the Universe, using the Bayesian inference method by defining the log-likelihood function

$$\ln \mathcal{L} = -\frac{1}{2} \ln \left( (2\pi)^N \det \mathbf{Cov} \right) - \frac{1}{2} \Delta \boldsymbol{\mu}^\top \mathbf{Cov}^{-1} \Delta \boldsymbol{\mu}, \quad (12)$$

where the distance modulus difference vector is

$$\Delta \boldsymbol{\mu} = \boldsymbol{\mu}_{\text{HII}}(\alpha, \kappa; \mathbf{z}_{\text{HII}}) - \boldsymbol{\mu}_{\text{OHD}}^{\text{rec}}(H_0, \Omega_{k0}; \mathbf{z}_{\text{HII}}), \quad (13)$$

and the corresponding total covariance matrix is

$$\mathbf{Cov} = \mathbf{Cov}_{\boldsymbol{\mu}_{\text{OHD}}^{\text{rec}}} + \text{diag}(\sigma_{\boldsymbol{\mu}_{\text{HII}}}^2), \quad (14)$$

where  $\mathbf{Cov}_{\boldsymbol{\mu}_{\text{OHD}}^{\text{rec}}}$  is covariance matrix of the reconstructed  $\boldsymbol{\mu}_{\text{OHD}}$  that described in eq. (10), while the covariance matrix of  $\boldsymbol{\mu}_{\text{HII}}$  is diagonal that described in eq. (5).

### 3. LOCAL MEASUREMENT THE $H_0$

In cosmography, the  $D_L(z)$ , as a function of redshift, can be expanded into the Taylor series as

$$D_L(z) = \frac{cz}{H_0} \left[ \mathcal{D}_L^0 + \mathcal{D}_L^1 z + \mathcal{D}_L^2 z^2 + \mathcal{O}(z^3) \right], \quad (15)$$

where

$$\begin{aligned} \mathcal{D}_L^0 &= 1 \\ \mathcal{D}_L^1 &= -\frac{1}{2}(1 - q_0) \\ \mathcal{D}_L^2 &= -\frac{1}{6}(1 - q_0 - 3q_0^2 + j_0). \end{aligned} \quad (16)$$

The  $q_0$  and  $j_0$  in above equation are the deceleration parameter the jerk parameter respectively, which are the dimensionless second and third derivative of the scale factor  $a(t)$  with respect to cosmic time  $t_0$ . And the first-order approximation at low redshifts in eq. (15) is the famous Hubble's law,

$$D_L(z) = \frac{cz}{H_0}. \quad (17)$$

It is independent of the mass-energy content of the Universe but only valid locally ( $z \lesssim 0.1$ ).

#### 3.1. Measurement with the Calibrated HIIGx Hubble Diagram

Once the Hubble diagram of HIIGx had been properly calibrated, it could be widely used to constrain cosmological model parameters. For instance, the  $H_0$  could be constrained directly using only the local HIIGx measurements, or it could be constrained together with energy density parameters using the entire sample and assuming a cosmological model. We will concentrate on the direct measurement of  $H_0$  in this article, which can be achieved by performing a Markov Chain Monte Carlo (MCMC) to maximize the log-likelihood function that described in eq. (12) with

$$\Delta \boldsymbol{\mu} = \boldsymbol{\mu}_{\text{HII}}^{\text{local}}(\alpha, \kappa; \mathbf{z}_{\text{HII}}^{\text{local}}) - \boldsymbol{\mu}_{\text{th}}(H_0; \mathbf{z}_{\text{HII}}^{\text{local}}), \quad (18)$$

where the theoretical  $H_0$ -dependent distance module  $\boldsymbol{\mu}_{\text{th}}(H_0, \mathbf{z}_{\text{HII}}^{\text{local}})$  is determined by substituting eq. (17) into eq. (3) at local redshifts ( $z < 0.1$ ) of HIIGx, and the corresponding covariance matrix is sub-matrix of the full  $\mathbf{Cov}_{\boldsymbol{\mu}_{\text{OHD}}^{\text{rec}}}$ ,

$$\mathbf{Cov} = \mathbf{Cov}_{\boldsymbol{\mu}_{\text{OHD}}^{\text{rec}}}(\mathbf{z}_{\text{HII}}^{\text{local}}, \mathbf{z}_{\text{HII}}^{\text{local}}). \quad (19)$$

To achieve a better constraint on the  $H_0$  and the calibration of the HIIGx Hubble diagram, we make a joint constraint by maximizing the summation of the log-likelihood function

$$\begin{aligned} \ln \mathcal{L} &= \ln \mathcal{L}(\boldsymbol{\mu}_{\text{HII}}, \boldsymbol{\mu}_{\text{OHD}}^{\text{rec}} | H_0, \Omega_{k0}, \alpha, \kappa) \\ &\quad + \ln \mathcal{L}(\boldsymbol{\mu}_{\text{HII}}^{\text{local}} | H_0, \alpha, \kappa) \end{aligned} \quad (20)$$

which are described in section 2 and here above.

#### 3.2. Measurement with the Cross-Calibrated SNe Hubble Diagram

SNe Ia is widely used as secondary standard candles to measure luminosity distances  $D_L$  because the peak luminosities of light curves of all SNe Ia are nearly identical. By identifying an SNe Ia that shares a host galaxy with a Cepheid variable, one can determine the host galaxy's  $D_L$  via its period-luminosity relation. Principally, by

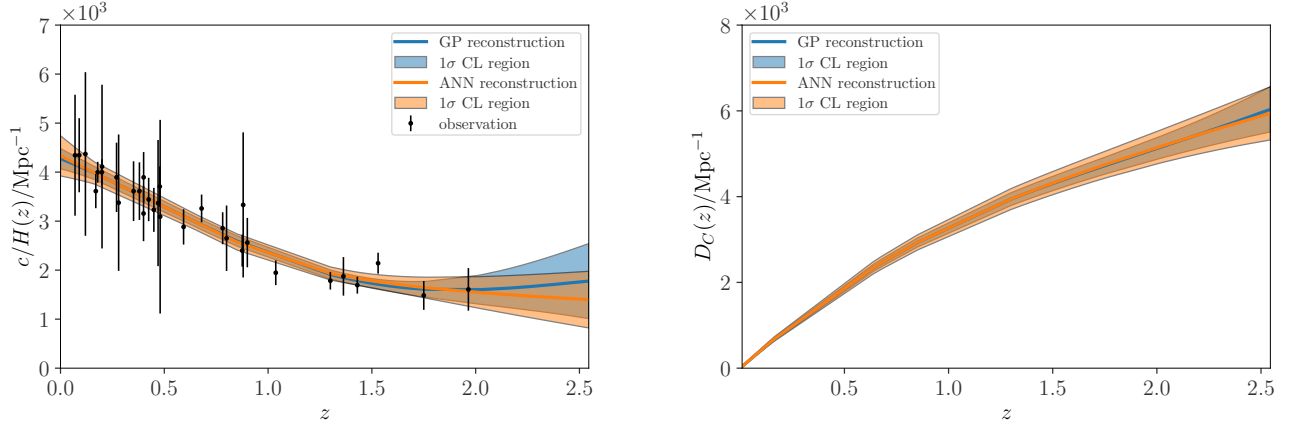


**Figure 1.** Left: reconstructions of  $c/H(z)$  using Gaussian Process (blue) and Artificial Neural Network (orange). The solid central lines represent the reconstructed values, whereas the shaded regions represent the  $1\sigma$  confidence intervals. The black error bars are the 32 OHD that are used as the basis in our reconstructions. Right: the corresponding reconstructions of the comoving distances, while  $1\sigma$  regions are calculated based on the upper and lower bounds of the  $c/H(z)$  in the left panel.

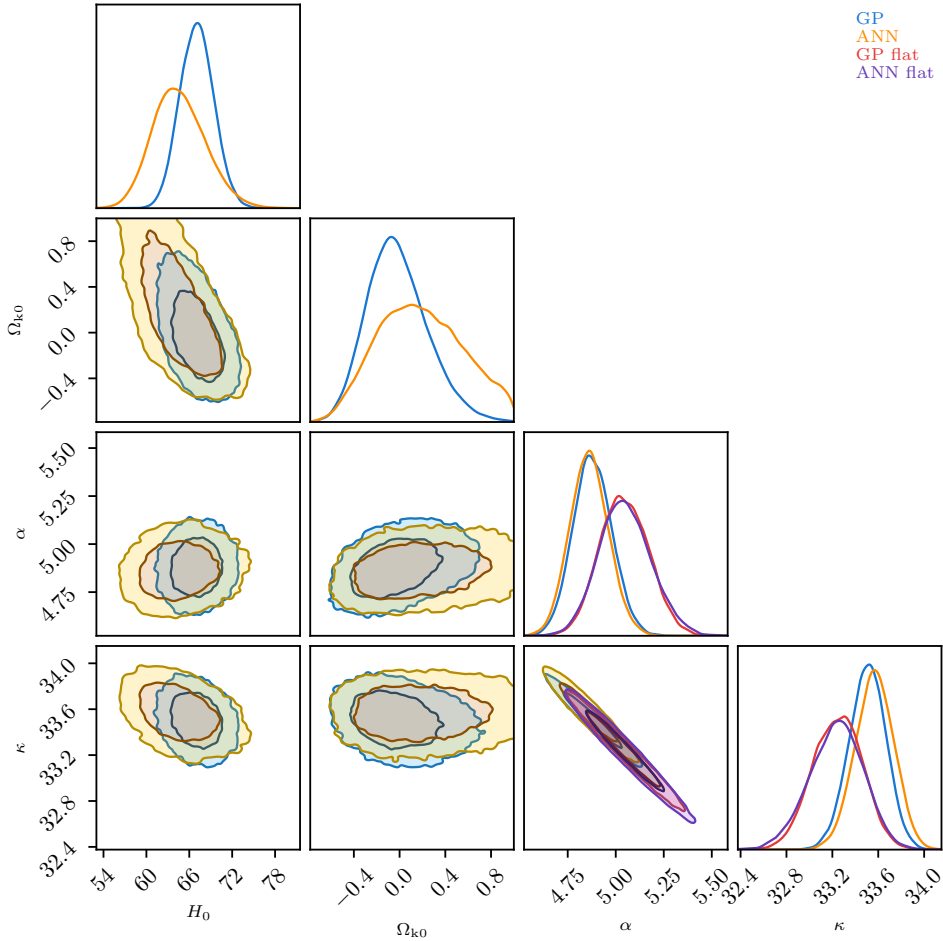


**Figure 2.** 68% and 95% confidence contours for the parameters involved in calibrating the HIIGx Hubble diagram with OHD. Results from the fit of not assuming flat Universe are show in blue and orange contours for using the GP and ANN reconstructed  $\mu_{\text{OHD}}$  data respectively, whereas the red and violet contours are that from the assuming a flat Universe.

combining the  $D_L$  with the peak apparent magnitude  $m_{\text{max}}$  of the SNe Ia, we can obtain the peak absolute

magnitude  $M_{\max}$  of all the SNe Ia using

$$\mu = 5 \lg \frac{D_L}{\text{Mpc}} + 25 = m_{\max} - M_{\max}. \quad (21)$$

Then the  $D_L$  of an arbitrary SNe Ia can be easily obtained by measuring its  $m_{\max}$ .

However, the  $M_{\max}$  of SNe Ia are not identical but also related to the shapes can colors of the light curves. Taking this into account, the formula for SNe Ia distance modulus should be modified by including perturbations of shapes  $x$  and color  $c$  as shown in [Guy et al. \(2007\)](#),

$$\mu_B(\alpha_X, \beta, M_B) = m_B^{\max} - M_B + \alpha_X X - \beta C, \quad (22)$$

where the subscript  $B$  stands for B band, while  $\alpha$  and  $\beta$  are nuisance parameters for modification. It is well known that the  $M_B$  is strongly correlated with  $H_0$ . As a convention in SNe Ia cosmology, it is safe to constrain parameters that are not very much dependent on  $M_B$ , based on an assumed value of  $H_0 = 70 \text{ km s}^{-1} \text{ Mpc}^{-1}$ . However, if the objective is to precisely measure the  $H_0$ , we must first obtain an accurate measurement of the  $M_B$ , which should also be modified according to the stellar mass ( $M_{\text{stellar}}$ ), in a step function form of

$$M_B = \begin{cases} M_B^1 & \text{if } M_{\text{stellar}} < 10^{10} M_{\odot} \\ M_B^1 + \Delta_M & \text{otherwise.} \end{cases}, \quad (23)$$

where the modified term  $\Delta_M$  only takes effect for massive objects. The eq. (22) can be written in matrix form of

$$\boldsymbol{\mu}_B = \mathbf{A}\boldsymbol{\eta} - M_B, \quad (24)$$

where the light-curve parameters vector is

$$\boldsymbol{\eta} = (m_{B1}, X_1, C_1, \dots, m_{Bn}, X_n, C_n), \quad (25)$$

and the coefficient matrix is

$$\mathbf{A} = \mathbf{A}_0 + \alpha \mathbf{A}_1 - \beta \mathbf{A}_2, \quad (26)$$

whose elements can be decide according to

$$(\mathbf{A}_k)_{i,j} = \delta_{3i,j+k}. \quad (27)$$

The covariance matrix of the  $\boldsymbol{\eta}$  consists of statistical uncertainties of light-curve fitting and seven sources of systematic uncertainties, including the covariance of calibration, light curve model, bias correction, mass step uncertainty, Milky Way dust extinction correction, peculiar velocity corrections, contamination of Hubble diagram by non-Ia. For detail descriptions please referred to [Betoule et al. \(2014\)](#). The covariance further propagate to  $\boldsymbol{\mu}_B$  in the form of

$$\text{Cov}_{\boldsymbol{\mu}_B} = \mathbf{A} \text{Cov}_{\boldsymbol{\eta}} \mathbf{A}^{\top} + \text{diag} \left( \frac{5\sigma_z}{z \ln 10} \right)^2 + \text{diag} (\sigma_{\text{lens}}^2) + \text{diag} (\sigma_{\text{coh}}^2), \quad (28)$$

taking account of the uncertainty in cosmological redshift due to peculiar velocities ( $\sigma_z$ ), the variation of magnitudes caused by gravitational lensing ( $\sigma_{\text{lens}}$ ), and the intrinsic variation in SN magnitude not described by the other terms ( $\sigma_{\text{coh}}$ ).

Once we get the HIIGx Hubble diagram which is precisely calibrated using the method described in section 2, we can take distance anchors from it to cross calibrate the SNe Ia Hubble diagram. We define the log-likelihood function in eq. (12) with the distance modulus difference vector in the form of

$$\Delta \boldsymbol{\mu} = \boldsymbol{\mu}_B(\alpha_x, \beta, M_B^1, \Delta M; \mathbf{z}_{\text{SNe}}) - \boldsymbol{\mu}_{\text{HII}}^{\text{rec}}(\mathbf{z}_{\text{SNe}}), \quad (29)$$

where  $\boldsymbol{\mu}_{\text{HII}}^{\text{rec}}(\mathbf{z}_{\text{SNe}})$  is reconstructed based on the calibrated  $\boldsymbol{\mu}_{\text{HII}}^{\text{calib}}$  described in section 2, whose error propagation is given by

$$\sigma_{\boldsymbol{\mu}_{\text{HII}}^{\text{calib}}}^2 = 2.5^2 [\alpha^2 \sigma_{\lg \sigma}^2 + \sigma_{\alpha}^2 \lg^2 \sigma + \sigma_{\kappa}^2 + \sigma_{\lg F}^2], \quad (30)$$

where  $\sigma_{\alpha}$ ,  $\sigma_{\kappa}$ , are the calibration errors of  $\alpha$  and  $\kappa$ , while  $\sigma_{\lg \sigma}$ ,  $\sigma_{\lg F}$  are measurement errors of  $\lg \sigma(\text{H}\beta)$  and  $\lg F(\text{H}\beta)$  respectively. The total covariance matrix corresponding to eq. (29) is

$$\mathbf{Cov} = \mathbf{Cov}_{\boldsymbol{\mu}_B} + \mathbf{Cov}_{\boldsymbol{\mu}_{\text{HII}}^{\text{rec}}}. \quad (31)$$

We take the same procedure in section 3.1 to determine the value of  $H_0$  using this cross calibrated SNe Hubble diagram, therefore we define

$$\Delta \boldsymbol{\mu} = \boldsymbol{\mu}_B^{\text{local}}(\alpha_x, \beta, M_B^1, \Delta M; \mathbf{z}_{\text{SNe}}^{\text{local}}) - \boldsymbol{\mu}_{\text{th}}(H_0; \mathbf{z}_{\text{SNe}}^{\text{local}}) \quad (32)$$

only using the local samples and get the covariance matrix

$$\mathbf{Cov} = \mathbf{Cov}_{\boldsymbol{\mu}_{\text{HII}}^{\text{rec}}}(\mathbf{z}_{\text{SNe}}^{\text{local}}, \mathbf{z}_{\text{SNe}}^{\text{local}}) \quad (33)$$

correspondingly. We perform a MCMC to maximize the summation of the log-likelihood function

$$\ln \mathcal{L} = \ln \mathcal{L}(\boldsymbol{\mu}_B, \boldsymbol{\mu}_{\text{HII}}^{\text{rec}} | \alpha_x, \beta, M_B^1, \Delta M) + \ln \mathcal{L}(\boldsymbol{\mu}_B^{\text{local}} | H_0, \alpha_x, \beta, M_B^1, \Delta M) \quad (34)$$

and get the  $H_0$  and calibrated SNe Hubble diagram simultaneously.

#### 4. DATA AND RESULTS

We applied the methods that are described in section 2 and 3 to the following list of data in detail.

- (1) *OHD*. We take the updated full sample of cosmological model-independent OHD which are measured according the equation

$$H(z) = -\frac{1}{1+z} \frac{dz}{dt} \simeq -\frac{1}{1+z} \frac{\Delta z}{\Delta t} \quad (35)$$

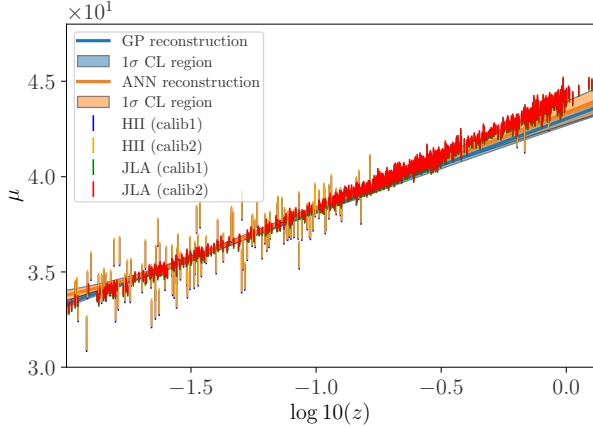


**Figure 3.** Hubble diagrams of HIIGx and JLA SNe Ia samples. Error-bars represent the calibrated distance modulus of the HIIGx and JLA sample and their corresponding  $1\sigma$  uncertainties, labeled by the sample names and calibration methods, with calib1 and calib2 stand for using Gaussian Process (GP) and Artificial Neural Network (ANN) reconstructed data respectively. The blue (orange) solid curves and shaded regions are the GP (ANN) reconstructed  $\mu_{\text{HII}}^{\text{rec}}$  and their corresponding  $1\sigma$  confidence regions at the redshift of JLA sample.

by measuring the time derivative of redshift  $dz/dt$  without assuming any cosmological model. The derivative is measured by taking the differential age of two massive and passively evolving galaxies at different redshifts as an approximation. A total number of 32 OHD (listed in table 1) are given by Jimenez et al. (2003); Simon et al. (2005); Stern et al. (2010); Moresco et al. (2012); Zhang et al. (2014); Moresco (2015); Moresco et al. (2016); Ratsimbazafy et al. (2017); Borghi et al. (2022); Jiao et al. (2022). Considering the last two measurements are not fully independent because they are derived from the same sample of passive galaxies sample, and their covariance is not clear yet, we decide only use the latest Jiao et al. (2022) measurement taking advantage of  $\sim 1/\sqrt{2}$  fraction of systematic uncertainty that is improved by approximately double number galaxies were used. One could either use the Borghi et al. (2022) measurement or both of them if the covariance is cleverly considered.

- (2) *HIIGx*. We use the full sample of HIIGx composed by González-Morán et al. (2021), which includes 107 local HII galaxies (Chávez et al. 2014) recalibrated by (González-Morán et al. 2019) in the redshift range of  $0.0088 \leq z \leq 0.16417$ , and 74 high- $z$  HII galaxies in the redshift range of  $0.63427 \leq z \leq 2.545$ . The fluxes and gas veloc-

ity dispersions (along with their uncertainties) of HIIGx and GEHR that we use in this article are all referred to from this catalogue.

- (3) *JLA*. This SNe Ia catalog is composed by Betoule et al. (2014) from observations obtained by the SDSS-II and SNLS collaborations. The data set includes several low-redshift samples ( $z < 0.1$ ), all three seasons from the SDSS-II ( $0.05 < z < 0.4$ ), and three years from SNLS ( $0.2 < z < 1$ ), and it totals 740 spectroscopically confirmed SNe Ia with high quality light curves. The light curve parameters ( $m_{B1}, X_1, C_1, \dots, m_{Bn}, X_n, C_n$ ) and the corresponding covariance matrix are all obtained from this catalogue.

For the calibration of the HIIGx Hubble diagram, we reconstruct  $D_C$  at the redshifts of HIIGx sample based on the OHD, whereas for the calibration of the JLA SNe Ia Hubble diagram we reconstruct  $\mu_{\text{HII}}$  at redshifts of JLA sample based on the pre-calibrated HIIGx Hubble diagram. We perform the following two methods to test the reliability of reconstructions. GP reconstructs values that are connected in each pair of data points by assuming a covariance function  $k(z, \tilde{z})$ . We use GAPP (Seikel et al. 2012) and adopt the squared exponential kernel function

$$k(z, \tilde{z}) = \sigma_f^2 \exp\left(-\frac{(z - \tilde{z})^2}{2\ell^2}\right), \quad (36)$$

where the signal variance  $\sigma_f$  and length scale  $\ell$  are two hyperparameters that should be optimized. The covariance matrix

$$\text{Cov} = \mathbf{K}_{**} - \mathbf{K}_{o*}^\top \mathbf{K}_{oo}^{-1} \mathbf{K}_{o*}, \quad (37)$$

where the subscripts  $o$  and  $*$  stand for calculating eq. (36) at the redshifts of the observational data and the reconstructed data, with the first and second position stand for the rows and columns respectively. ANN is an alternative non-parametrical reconstruction method free of assumptions that can improve reliability. We use REFANN as our second tool, which is validated in reconstructing OHD and  $D_L(z)$  (Wang et al. 2020b). The covariance matrix of can be estimated by the method described in section 6.2 of Wang et al. (2020b),

$$\text{Cov}\left(\frac{c}{\bar{H}_i}, \frac{c}{\bar{H}_j}\right) = \frac{1}{N} \sum_{k=1}^N \left[ \left( \frac{c}{\bar{H}_i k} - \frac{\bar{c}}{\bar{H}_i} \right) \left( \frac{c}{\bar{H}_j k} - \frac{\bar{c}}{\bar{H}_j} \right) \right], \quad (38)$$

which averaged over a large number of reconstructions (i.e.,  $N = 1000$ ) based on Gaussian re-sampling of the observational data. We reconstruct solely within the intercept redshift interval shared by the basis data and

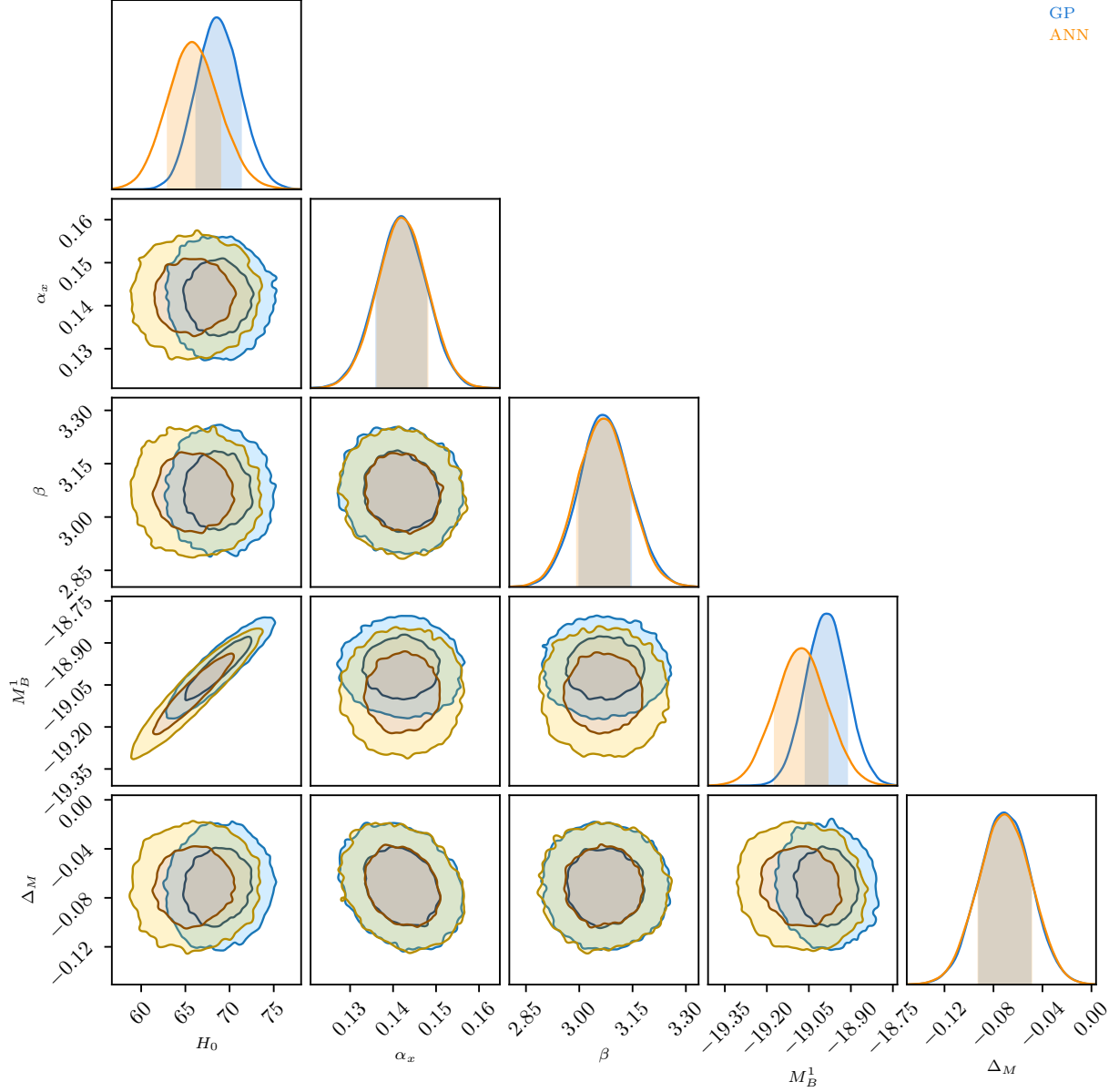


**Figure 4.** 68% and 95% confidence contours for the parameters involved in calibrating the SNe Hubble diagram with calibrated HIIGx data. Blue (orange) contours result from the fit of using the GP (ANN) reconstructed  $\mu_{\text{HI}}$  data and the full JLA sample.

the data for comparison in our Bayesian analysis, considering that interpolation is more trustworthy than extrapolation.

In Figure 1 we show the reconstructed  $c/H(z)$  and  $D_C(z)$  which are based on the OHD. The GP and ANN behave different on  $c/H(z)$  reconstruction at both lower and higher end of the redshift range, which result to the difference of the  $D_C(z)$ . Based on the reconstruction, we calibrate the HIIGx Hubble diagram without assuming the flatness of the Universe and show the involved parameters in Figure 2 and their summary in Table 2. We observe inverse correlation ( $r \sim -0.49$ ) between  $H_0$  and  $\Omega_k$ , which is known as the geometry degeneracy.

We also observe strong inverse correlation ( $r \sim -0.98$ ) between  $\alpha$  and  $\kappa$ . The correlation between the cosmic parameters and the calibration coefficients should not be overlooked, especially for the correlation between  $\Omega_{k0}$  and  $\alpha$  that shows correlation coefficient  $r \sim 0.36$ . As a comparison result, we also show the calibration coefficients from assuming a flat Universe and find  $1.07 \sigma$  and  $1.14 \sigma$  difference between the two set of  $\alpha$  and  $\kappa$  respectively.

We show the OHD calibrated HIIGx Hubble diagrams and their reconstructions in Figure 3, companion with the calibrated JLA SNe Ia Hubble diagrams based on the reconstructed data. The calibration parameters and

**Table 1.** All the Observational  $H(z)$  Data derived from the Cosmic Chronometers (CC) method

$z$	$H(z)$	$\sigma_H$	References
0.09	69	12	Jimenez et al. (2003)
0.17	83	8	
0.27	77	14	
0.4	95	17	
0.9	117	23	Simon et al. (2005)
1.3	168	17	
1.43	177	18	
1.53	140	14	
1.75	202	40	
0.48	97	62	Stern et al. (2010)
0.88	90	40	
0.1791	75	4	
0.1993	75	5	
0.3519	83	14	
0.5929	104	13	Moresco et al. (2012)
0.6797	92	8	
0.7812	105	12	
0.8754	125	17	
1.037	154	20	
0.07	69	19.6	
0.12	68.6	26.2	Zhang et al. (2014)
0.2	72.9	29.6	
0.28	88.8	36.6	
1.363	160	33.6	Moresco (2015)
1.965	186.5	50.4	
0.3802	83	13.5	
0.4004	77	10.2	
0.4247	87.1	11.2	Moresco et al. (2016)
0.4497	92.8	12.9	
0.4783	80.9	9	
0.47	89	34	Ratsimbazafy et al. (2017)
0.75	98.8	33.6	Borghi et al. (2022)
0.80	113.1	28.5	Jiao et al. (2022)

\*  $H(z)$  and  $\sigma_H$  are in the unit of  $\text{km s}^{-1} \text{Mpc}^{-1}$

the jointly constrained  $H_0$  are shown in Figure 4 and summarised in Table 2. We observe strong correlation ( $r \sim 0.92$ ) between  $H_0$  and  $M_B^1$ .

## 5. CONCLUSION AND DISCUSSION

Cosmic Chronometers (also known as OHD) can be used as distance anchors to constrain the  $L - \sigma$  relation

coefficients of the HII Galaxies, therefore provide us an alternative cosmological-model independent method to calibrate the HIIGx Hubble diagram. We promote this method by removing the flat Universe assumption and observe weak correlations between the cosmic parameters ( $H_0$  and  $\Omega_{k0}$ ) and the coefficients ( $\alpha$  and  $\kappa$ ). We observe approximately  $1 \sigma$  difference between the calibrations assuming or not the flatness of the Universe. This indicates the necessity of assumption-free for improving the reliability of the calibration.

We implement a non-parametric Artificial Neural Network method for reconstructing data in the intermediate process of calibration and obtain  $\alpha = 4.861^{+0.101}_{-0.099}$  and  $\kappa = 33.57 \pm 0.17$  with its reliability affirmed by highly compatible Gaussian Process involved result. We obtain Hubble constant with a value of  $H_0 = 64.4^{+3.9}_{-3.4} \text{ km s}^{-1} \text{Mpc}^{-1}$ , which is lower but still compatible with the Planck18 measurement ( $H_0 = 67.4 \pm 0.5 \text{ km s}^{-1} \text{Mpc}^{-1}$ , Planck Collaboration et al. (2020)).

We calibrate the JLA SNe Ia Hubble diagram using the calibrated HIIGx Hubble diagram as an anchor, making it possible to be free of the conventional assumption of  $H_0 = 70 \text{ km s}^{-1} \text{Mpc}^{-1}$ . The newly calibrated JLA Hubble diagram can be used to constrain any cosmological parameters including those degenerated with the  $H_0$ . We obtain a jointly constrained value of  $H_0 = 65.9^{+3.0}_{-2.9} \text{ km s}^{-1} \text{Mpc}^{-1}$ , which is more compatible with the Planck18 measurement than what we get from the HIIGx Hubble diagram.

In conclusion, our method further improves the reliability of the HIIGx Hubble diagram calibrated with OHD by removing the assumption of cosmological flatness in the method of Wu et al. (2020) and the assumption of kernel functions in the reconstruction. This method can be used to obtain cosmological-model independent calibrations of other Hubble diagrams.

- 1 We appreciate the referee's several useful suggestions, as
- 2 well as Guo-Jian Wang's kindly instruction about the
- 3 *ReFANN*. We also thank Yu-Chen Wang, Yun-Long Li
- 4 and Cheng-Zong Ruan for valuable discussions. This
- 5 work is supported by the National Science Foundation
- 6 of China(Grants Nos. 61802428, 11929301). Kang Jiao
- 7 is also funded by the China Scholarship Council (CSC)
- 8 from the Ministry of Education of P.R. China.

*Software:* GAPP (Seikel et al. 2012), REFANN (Wang et al. 2020b), EMCEE (Foreman-Mackey et al. 2013), CHAINCONSUMER (Hinton 2016), NUMPY (Harris et al. 2020), SCIPY (Virtanen et al. 2020), MATPLOTLIB (Hunter 2007).

**Table 2.** Calibration Parameters of Hubble Diagrams.

HIIGx	$H_0$	$\Omega_{k0}$	$\alpha$	$\kappa$	
OHD+GP	$67.0 \pm 2.4$	$-0.04^{+0.29}_{-0.24}$	$4.877^{+0.103}_{-0.098}$	$33.51 \pm 0.16$	
OHD+ANN	$64.4^{+3.9}_{-3.4}$	$0.17^{+0.42}_{-0.37}$	$4.861^{+0.101}_{-0.099}$	$33.57 \pm 0.17$	
SNe	$H_0$	$\alpha_x$	$\beta$	$M_B^1$	$\Delta M$
HII+GP	$68.7^{+2.6}_{-2.5}$	$0.1419 \pm 0.0058$	$3.071^{+0.074}_{-0.070}$	$-18.987^{+0.073}_{-0.074}$	$-0.071 \pm 0.021$
HII+ANN	$65.9^{+3.0}_{-2.9}$	$0.1422 \pm 0.0058$	$3.068 \pm 0.073$	$-19.078^{+0.094}_{-0.093}$	$-0.071 \pm 0.021$

NOTE— Parameters are the summaries of the Figure 2 and 4.  $H(z)$  is in the unit of  $\text{km s}^{-1} \text{Mpc}^{-1}$ .

## REFERENCES

- Betoule, M. e. a., Kessler, R., Guy, J., et al. 2014, A&A, 568, A22, doi: [10.1051/0004-6361/201423413](https://doi.org/10.1051/0004-6361/201423413)
- Borghi, N., Moresco, M., & Cimatti, A. 2022, ApJL, 928, L4, doi: [10.3847/2041-8213/ac3fb2](https://doi.org/10.3847/2041-8213/ac3fb2)
- Chávez, R., Terlevich, E., Terlevich, R., et al. 2012, MNRASL, 425, L56, doi: [10.1111/j.1745-3933.2012.01299.x](https://doi.org/10.1111/j.1745-3933.2012.01299.x)
- Chávez, R., Terlevich, R., Terlevich, E., et al. 2014, MNRAS, 442, 3565, doi: [10.1093/mnras/stu987](https://doi.org/10.1093/mnras/stu987)
- Demianski, Marek, Piedipalumbo, Ester, Sawant, Disha, & Amati, Lorenzo. 2017, A&A, 598, A112, doi: [10.1051/0004-6361/201628909](https://doi.org/10.1051/0004-6361/201628909)
- Fernández Arenas, D., Terlevich, E., Terlevich, R., et al. 2017, MNRAS, 474, 1250, doi: [10.1093/mnras/stx2710](https://doi.org/10.1093/mnras/stx2710)
- Foreman-Mackey, D., Hogg, D. W., Lang, D., & Goodman, J. 2013, PASP, 125, 306, doi: [10.1086/670067](https://doi.org/10.1086/670067)
- González-Morán, A. L., Chávez, R., Terlevich, R., et al. 2019, MNRAS, 487, 4669, doi: [10.1093/mnras/stz1577](https://doi.org/10.1093/mnras/stz1577)
- González-Morán, A. L., Chávez, R., Terlevich, E., et al. 2021, MNRAS, 505, 1441, doi: [10.1093/mnras/stab1385](https://doi.org/10.1093/mnras/stab1385)
- Guy, J., Astier, P., Baumont, S., et al. 2007, A&A, 466, 11, doi: [10.1051/0004-6361:20066930](https://doi.org/10.1051/0004-6361:20066930)
- Harris, C. R., Millman, K. J., van der Walt, S. J., et al. 2020, Nature, 585, 357, doi: [10.1038/s41586-020-2649-2](https://doi.org/10.1038/s41586-020-2649-2)
- Hinton, S. R. 2016, The Journal of Open Source Software, 1, 00045, doi: [10.21105/joss.00045](https://doi.org/10.21105/joss.00045)
- Hunter, J. D. 2007, Computing in Science Engineering, 9, 90, doi: [10.1109/MCSE.2007.55](https://doi.org/10.1109/MCSE.2007.55)
- Jiao, K., Borghi, N., Moresco, M., & Zhang, T.-J. 2022, arXiv e-prints, arXiv:2205.05701. <https://arxiv.org/abs/2205.05701>
- Jimenez, R., Verde, L., Treu, T., & Stern, D. 2003, ApJ, 593, 622, doi: [10.1086/376595](https://doi.org/10.1086/376595)
- Kumar, P., & Linder, E. V. 2019, PRD, 100, 083533, doi: [10.1103/PhysRevD.100.083533](https://doi.org/10.1103/PhysRevD.100.083533)
- Leaf, K., & Melia, F. 2018, MNRAS, 474, 4507, doi: [10.1093/mnras/stx3109](https://doi.org/10.1093/mnras/stx3109)
- Lusso, E., & Risaliti, G. 2017, A&A, 602, A79, doi: [10.1051/0004-6361/201630079](https://doi.org/10.1051/0004-6361/201630079)
- Lusso, E., Risaliti, G., Nardini, E., et al. 2020, A&A, 642, A150, doi: [10.1051/0004-6361/202038899](https://doi.org/10.1051/0004-6361/202038899)
- Melnick, J., Telles, E., Bordalo, V., et al. 2017, A&A, 599, A76, doi: [10.1051/0004-6361/201629728](https://doi.org/10.1051/0004-6361/201629728)
- Mishra, A., Reddy, P., & Nigam, R. 2019, CMB-GAN: Fast Simulations of Cosmic Microwave background anisotropy maps using Deep Learning
- Moresco, M. 2015, MNRAS, 450, L16, doi: [10.1093/mnrasl/slv037](https://doi.org/10.1093/mnrasl/slv037)
- Moresco, M., Verde, L., Pozzetti, L., Jimenez, R., & Cimatti, A. 2012, JCAP, 7, 053, doi: [10.1088/1475-7516/2012/07/053](https://doi.org/10.1088/1475-7516/2012/07/053)
- Moresco, M., Pozzetti, L., Cimatti, A., et al. 2016, JCAP, 5, 014, doi: [10.1088/1475-7516/2016/05/014](https://doi.org/10.1088/1475-7516/2016/05/014)
- Mustafa, M., Bard, D., Bhimji, W., et al. 2019, CompAC, 6, 1, doi: [10.1186/s40668-019-0029-9](https://doi.org/10.1186/s40668-019-0029-9)
- Peel, A., Lalande, F., Starck, J.-L., et al. 2019, PRD, 100, 023508, doi: [10.1103/PhysRevD.100.023508](https://doi.org/10.1103/PhysRevD.100.023508)
- Perlmutter, S., Aldering, G., Goldhaber, G., et al. 1999, ApJ, 517, 565, doi: [10.1086/307221](https://doi.org/10.1086/307221)
- Planck Collaboration, Aghanim, N., Akrami, Y., et al. 2020, A&A, 641, A6, doi: [10.1051/0004-6361/201833910](https://doi.org/10.1051/0004-6361/201833910)
- Ratsimbazafy, A. L., Loubser, S. I., Crawford, S. M., et al. 2017, MNRAS, 467, 3239, doi: [10.1093/mnras/stx301](https://doi.org/10.1093/mnras/stx301)

- Riess, A. G., Filippenko, A. V., Challis, P., et al. 1998, *AJ*, 116, 1009, doi: [10.1086/300499](https://doi.org/10.1086/300499)
- Salvestrini, F., Risaliti, G., Bisogni, S., Lusso, E., & Vignali, C. 2019, *A&A*, 631, A120, doi: [10.1051/0004-6361/201935491](https://doi.org/10.1051/0004-6361/201935491)
- Schmelzle, J., Lucchi, A., Kacprzak, T., et al. 2017, *Cosmological model discrimination with Deep Learning*
- Seikel, M., Clarkson, C., & Smith, M. 2012, *JCAP*, 2012, 036, doi: [10.1088/1475-7516/2012/06/036](https://doi.org/10.1088/1475-7516/2012/06/036)
- Siegel, E. R., Guzmán, R., Gallego, J. P., López, M. O., & Hidalgo, P. R. 2005, *MNRAS*, 356, 1117, doi: [10.1111/j.1365-2966.2004.08539.x](https://doi.org/10.1111/j.1365-2966.2004.08539.x)
- Simon, J., Verde, L., & Jimenez, R. 2005, *PRD*, 71, 123001, doi: [10.1103/PhysRevD.71.123001](https://doi.org/10.1103/PhysRevD.71.123001)
- Stern, D., Jimenez, R., Verde, L., Kamionkowski, M., & Stanford, S. A. 2010, *JCAP*, 2, 008, doi: [10.1088/1475-7516/2010/02/008](https://doi.org/10.1088/1475-7516/2010/02/008)
- Terlevich, R., & Melnick, J. 1981, *MNRAS*, 195, 839, doi: [10.1093/mnras/195.4.839](https://doi.org/10.1093/mnras/195.4.839)
- Terlevich, R., Terlevich, E., Melnick, J., et al. 2015, *MNRAS*, 451, 3001, doi: [10.1093/mnras/stv1128](https://doi.org/10.1093/mnras/stv1128)
- Virtanen, P., Gommers, R., Oliphant, T. E., et al. 2020, *Nature Methods*, 17, 261, doi: [10.1038/s41592-019-0686-2](https://doi.org/10.1038/s41592-019-0686-2)
- Wang, G.-J., Li, S.-Y., & Xia, J.-Q. 2020a, *ApJS*, 249, 25, doi: [10.3847/1538-4365/aba190](https://doi.org/10.3847/1538-4365/aba190)
- Wang, G.-J., Ma, X.-J., Li, S.-Y., & Xia, J.-Q. 2020b, *ApJS*, 246, 13, doi: [10.3847/1538-4365/ab620b](https://doi.org/10.3847/1538-4365/ab620b)
- Wang, Y.-C., Xie, Y.-B., Zhang, T.-J., et al. 2021, *ApJS*, 254, 43, doi: [10.3847/1538-4365/abf8aa](https://doi.org/10.3847/1538-4365/abf8aa)
- Wei, J.-J., Wu, X.-F., & Melia, F. 2016, *MNRAS*, 463, 1144, doi: [10.1093/mnras/stw2057](https://doi.org/10.1093/mnras/stw2057)
- Wu, Y., Cao, S., Zhang, J., et al. 2020, *ApJ*, 888, 113, doi: [10.3847/1538-4357/ab5b94](https://doi.org/10.3847/1538-4357/ab5b94)
- Yennapureddy, M. K., & Melia, F. 2017, *JCAP*, 2017, 029, doi: [10.1088/1475-7516/2017/11/029](https://doi.org/10.1088/1475-7516/2017/11/029)
- Zhang, C., Zhang, H., Yuan, S., et al. 2014, *RAA*, 14, 1221, doi: [10.1088/1674-4527/14/10/002](https://doi.org/10.1088/1674-4527/14/10/002)